

Spectral, Electron Microscopical and Chemical Characteristics of the Gem-Quality Silica-Rich Rhodonite

MURAT HATIPOGLU

Dokuz Eylul University, IMYO, Izmir Multidisciplinary Vocational School, Gemmology and Jewellery Programme, 35380 Buca, Izmir, Turkey

Corresponding author: Tel: +90 232 4400707/107; E-mail: murat.hatipoglu@deu.edu.tr

(Received: 5 March 2011;

Accepted: 14 October 2011)

AJC-10518

Large-sized massive masses of gem-quality silica-rich Anatolian rhodonite occur as an element of the hydrothermal replacement mineralization paragenesis in the Menderes-Izmir region of Turkey. The samples display some distinctive cathodoluminescence and thermoluminescence spectral luminescence emissions. The cathodoluminescence AC graphics of the rhodonite samples at 14 keV energy and frequencies of 90 and 180 Hz after excited by electron irradiation at room temperature indicate that there are three major spectral emissions, the dominant one being in the middle visible wavelength region (nearly yellow) at about 600 nm. Additionally, two lesser emission lines occur in the longer visible wavelength region (nearly red) at about 670 nm and in the shorter visible wavelength region (nearly blue) at about 490 nm. On the other hand, the cathodoluminescence data at 24 keV energy and frequencies of 9 and 90 Hz indicate that one distinctive spectral emission in the visible wavelength region between yellow and orange is present at about 620 nm. Minor emissions also exist in the shorter visible wavelength region (nearly lavender-blue) at about 420 nm and in the ultraviolet wavelength region at about 315 nm. Meanwhile, the cathodoluminescence DC spectra at energies of 14 and 24 keV the rhodonite samples are similar to the AC graphics regarding their wavelength positions and intensities, although their values are higher. These are at about 615, 600, 570, 500, 490, 430, 425, 395 and 305 nm, from the longer visible wavelength region to the ultraviolet wavelength region. It can be claimed that dominant cathodoluminescence emissions in the visible region are due to some extrinsic defects (chemical impurities) (dominant band at around 600 nm) and the others intrinsic defects (the nonbridging oxygen deficient centres with several precursors and self-trapped exciton) (minor bands at around 500, 400 and 300 nm) since the intensities and positions of these emissions are significantly different at two various energies, being due to increasing amounts of tetrahedral character with increasing electron density due to the presence of trace elements, taking into consideration the increased ionic character of the Si-O bond in the manganese silicate. The thermoluminescence glow curves of the rhodonite sample after X-ray beams for different irradiation times (10, 20 and 30 min) in temperatures ranging from 50-400 °C display two main peaks which are observed at about 143 and 300 °C. Even if raised to the maximum dose, the behaviour of the thermoluminescence curves remains nearly stable, but their intensities increase. Major cathodoluminescence emissions appearing at the yellow-orange region at around 600 nm suggest that the Anatolian rhodonite may have arisen from a host with relatively lower levels of the basic building elements (Mg, Na, K, P and Ba) and is consequently richer in free silica and calcium, *i.e.*, of a more "neutral" character. However, some transition and rare earth elements (Fe, Mn, As, Bi, Cu, Ga, Pb, Tl, U and Zn) are significantly elevated. The presence of these major and minor cathodoluminescence and thermoluminescence emissions suggests that relatively higher levels of the transition elements can be attributed to a complicated geothermal system in the region.

Key Words: Rhodonite, XRD, XRF and ICP-AES, SEM, Cathodoluminescence, Thermoluminescence, Genesis, Paleo-temperature, Menderes-Izmir, Turkey.

INTRODUCTION

Even though the mineral rhodonite has its composition as MnSiO_3 ¹⁻⁵, formulas including more cations are already present, such as $\text{CaMn}_4\text{Si}_5\text{O}_{15}$ ⁶, $(\text{Mn,Ca})\text{SiO}_3$ ^{7,8} and $(\text{Mn,Ca,Fe,Mg})\text{SiO}_3$ ⁹. In addition, some special cation-rich rhodonite occurrences from worldwide localities have been reported, such as Mg-rich rhodonite^{10,11} and Zn-rich rhodonite¹². While some of the previously investigated and reported rhodonite occurrences are the specimens with typical crystalline shape,

the others are the massive masses without typical crystalline shape.

The gem-quality rhodonite occurrences from the Menderes-Izmir region of Turkey are massive-structured masses. They are rarely mentioned in the literature^{13,14}. Thus, the investigation of the luminescence features of such a rhodonite occurrence, which is an element of the hydrothermal replacement mineralization paragenesis in the metasomatic zone, can give us some interesting genetic data, which can be applied to other gems obtained from other localities.

Cathodoluminescence (CL), which is an optical and electrical phenomenon in which an electron beam is generated by a cathode ray tube and then impacts on potentially luminescent centres in a material, provides essential information on provenance, composition, growth fabrics, diagenetic textures, defects in the lattice and mineral zonation¹⁵. Peak width, peak position and transition probability of the luminescence centres are influenced by effects such as interactions within the defects themselves and interaction between defects and the surrounding crystal lattice^{16,17}. The actual cathodoluminescence colour is determined by the number and type of emission and quenching centres present. Super imposition of several luminescence bands of different intensities can provide quantitative data on the wavelength and intensity of luminescence and the nature of the luminescence centres^{15,18,19}.

The weak but highly variable cathodoluminescence colours and emission spectra of minerals, especially quartz, can be related to the genetic conditions of quartz formation. Hence, both luminescence microscopy and spectroscopy can be used widely in geosciences and various technical applications^{16,19}.

Thermoluminescence (TL) is a form of luminescence that is clearly exhibited by certain crystalline materials²⁰. In some crystalline materials, the electronically excited states which are created by high energy radiation are trapped, or arrested, for extended periods of time by localized defects or imperfections, in the lattice interrupting the normal intermolecular or inter-atomic interactions in the crystal lattice²⁰. Therefore, thermoluminescence is a very sensitive technique for the detection of traps or defects. Most ions at the surface are not saturated in coordination; electrons or holes may be excited easily and escape from the ions and then they are trapped at surface states located in the forbidden gap. When the sample is heated the detrapping of electrons and their subsequent recombination with holes gives rise to light emission. However, the situation will change if both electrons and holes are released from their traps at the same time at the same temperature interval and the holes are being thermally released from the same centres which act as recombination sites for the thermally released electrons and *vice versa*²¹.

A combined study of X-ray diffraction (XRD), chemical analyses (XRF and ICP-AES), scanning electron imaging (SEM), cathodoluminescence (CL) and thermoluminescence (TL) spectroscopy on the massive rhodonite samples can provide some essential mineralogical and geological data. Therefore, this study has three aims. (i) To investigate the individual luminescence patterns of the samples of Anatolian rhodonite. (ii) To determine information concerning the genesis of this mineral during hydrothermal replacement mineralization formations in the Menderes-Izmir region of Turkey. (iii) To demonstrate that cathodoluminescence (after excitement by electron irradiation) and thermoluminescence (after X-ray irradiation) spectral luminescence emissions can be used as an indicator for the provenance and paleo-temperature conditions of replacement mineralization yields.

EXPERIMENTAL

The investigated gem-quality rhodonite samples are an element of the secondary hydrothermal replacement

mineralisation paragenesis which occurred through the fracture zone of the vein-type epithermal gold deposit^{13,14} located in Efemçukuru village, near the Menderes district of Izmir in Turkey (Figs. 1A and B). Rhodonite mineralizations are embedded as large fracture-filling masses. It has been previously reported in the detailed geological and mining investigations by Baba and Güngör¹³ and Oyman *et al.*¹⁴ that the accompanying hydrothermal replacement minerals in the same metasomatic zone are mainly axinite, epidote, rhodochrosite and tephroite. The investigated rhodonite samples are pinkish and sometimes pinkish-red coloured compact masses of up to 80 cm with blackish dentrites, including prismatic to relatively thin tabular crystals, commonly in a blackish-grey coloured matrix of coarsely crystalline massive manganese oxides/hydroxides (Fig. 1C). The samples are found in the stockwork zone of the wall-rock hornfels and in the vein breccia and related metasomatic zone. Ultimately, these Anatolian rhodonite occurrences and related mineral paragenesis are hosted by the Late Cretaceous-Paleogene aged diagenetic flysch facies rocks of the Izmir-Ankara zone, which were intruded by rhyolites erupted by Neogene volcanism^{13,14}.

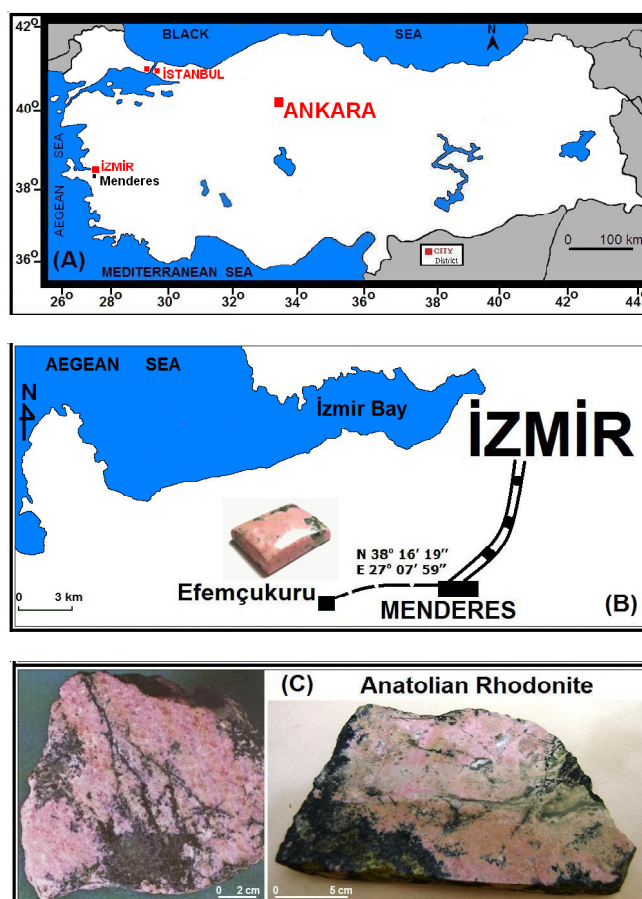


Fig. 1. Location map of the investigated samples, located in the Menderes-Izmir region of Turkey (A) and enlarged map (B). Gem-quality rhodonite samples occur as pinkish colored compact masses of up to 80 cm with blackish dentrites including prismatic to relatively thin tabular crystals, commonly in a blackish-grey colored matrix of coarsely crystalline massive manganese oxides (hydroxide). The samples are found in the stockwork zone of the wall-rock hornfels and in the vein breccia, as an element of the replacement mineralisation of the vein-type epithermal gold deposit in the diagenetic flysch rock and related metasomatic zone (C)

X-Ray diffractometry of the representative sample, which this sample most typical part in the deposit regarding with its appearance and colouration, was generated from its powder using a Rigaku MiniFlex X-ray Diffraction System, operating in ambient temperature at 40 keV and 30 mA. The initial and final wavelength analysis for the sample was performed using irradiation of CuK_α at a scanning rate of $0.33^\circ/\text{min}$ for 2θ from 0.000 - 70.000° . d-Spacing [\AA] diffraction matching was performed using a comparative matching technique based on the positions of peaks with relative intensities [$\% (I/I_0) \geq 10$] and 2θ values below 70° .

Chemical analyses of the representative sample utilized X-ray fluorescence (XRF) for major oxides, inductively coupled plasma-atomic emission spectroscopy (ICP-AES) for trace elements and WST-SIM to determine ignition losses. These analyses were performed and certified with the code number "IZ10057335", under contract by the accredited ALS Chemex Laboratory in Canada.

The scanning electron microscope (SEM) images of the representative sample were obtained using a Philips XL 30S FEG (Field Transmittance Gun) scanning electron microscope after the sample was coated with a 5 mm thick layer of gold powder. The images were recorded using the BSE (Back Scattered Electron) technique to show atom contrasts at 150x magnification and the SE (scattered electron) technique to show submicron structure at 150x, 5.000x, 10.000x, 20.000x, 50.000x and 100.000x magnifications.

Cathodoluminescence time resolved spectroscopy was performed on the representative sample. The acceleration potential was 24 keV and the current was 20 mA, corresponding to an incident power density of 0.8 mW cm^{-2} . The primary electron beam was pulsed using a Thandor TG501 5 MHz function generator set to a sine function with a frequency of 90 Hz, except for the lifetime measurement. The cathodoluminescence response was gated using an EgandG Ortholoc-SC 9505 2-phase lock-in amplifier. Spectra were measured at room temperature and energies of 14 and 24 keV using an f/4 scanning monochromator and a cooled red-sensitive photomultiplier tube. It is worth noting that the broad diameter of the beam significantly reduces any instability due to secondary electron emission. Two different measurements were performed, namely alternating current (AC) and direct current (DC). In AC measurement, an Ortholo-SC9505 two phase lock-in amplifier was employed. This instrument was used in normal mode, where it performs in exactly the same way as an ordinary lock-in amplifier, *i.e.*, only one channel is needed. Output from the PM tube is first fed into a Brook-deal 5002 current pre-amplifier mounted near to the tube. This pre-amplifier provides a more suitable input to lock-in, being able to sink a considerable DC current. Its output can be varied to provide the optimum amount of AC gain against DC reduction. All spectra were recorded from the lower to higher wavelengths. All spectra shown here have been corrected for system response. The electron beam was chopped at frequencies from 9-900 Hz and the photomultiplier output was measured on the lock-in amplifier. In most cases, the DC signal was satisfactory, for example, when there were strong lifetime effects at low chopping rates, the signals were such that the background noise from the PM tube

was negligible. The background proved to be of greater importance for DC measurements due to the reflection in the sample of light from the gun filament. Therefore, the cathodoluminescence response was studied as a function of intensities and wavelength or energy in both AC and DC measurements.

Thermoluminescence spectroscopy was performed on the representative sample. The X-ray irradiation was supplied by a Machlett OEG-50A tube. All irradiations were accomplished using a 30 Gy/min dose at room temperature. The thermoluminescence readouts were carried out from room temperature up to 400°C under N_2 atmosphere using a RA94 TLD Reader Analyser. The heating rate was 5°C/s .

RESULTS AND DISCUSSION

Gem-quality pinkish massive-structured Anatolian rhodonite occurrences (Fig. 1C) were investigated using X-ray diffraction pattern (XRD), instrumental chemical analyses (XRF and ICP-AES), scanning electron microscope photos (SEM) and two spectral luminescence techniques (cathodoluminescence and thermoluminescence), to find out the relationships between spectral luminescence emissions and crystalline (extrinsic and/or intrinsic) defects, which reflect the genesis conditions. Thus, the spectral luminescence profiles of the Anatolian rhodonite occurrences have been revealed for the first time.

In order to establish the exact inner structure of the sample, the numerical data obtained from the experimental XRD data of the sample were labelled on the X-ray diffraction pattern (Fig. 2). The d-spacing [\AA] diffraction values of the massive-structured fine-crystalline Anatolian rhodonite sample were matched with the d-spacing [\AA] diffraction values of the previously published single-crystalline rhodonite and α -quartz samples, compiled from the PDF Cards²² and some crystal structure databases²³⁻²⁵. As seen from the pattern, the Anatolian rhodonite occurrence has a rich α -quartz silica phase, which makes it slightly different to single-crystalline rhodonite occurrences from other worldwide localities⁵.

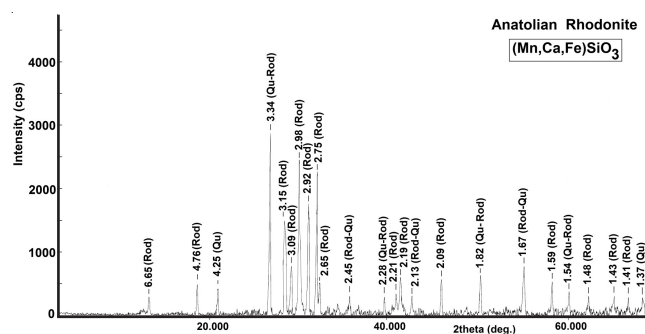


Fig. 2. X-Ray diffraction (XRD) pattern of the silica-rich massive Anatolian rhodonite sample from the Menderes-Izmir region in Turkey. Labels (Rod for rhodonite and Qu for alpha quartz) show the single and overlapping XRD peaks using the comparative matching technique according to the d-spacing [\AA] and relative intensities [$\% (I/I_0) \geq 10$] of the experimental XRD numerical data

Chemical analyses are one of the most important interpretation methods for the geochemical evaluation of metasomatic mineral formations and provenance characteristics¹¹. In addition, chemical impurities may be differently incorporated in crystals

TABLE-1
 CHEMICAL BULK AND TRACE ELEMENT ANALYSES OF THE ANATOLIAN RHODONITE FROM THE IZMIR-MENDERES REGION IN TURKEY, WHILE WAS DEPOSITED IN THE STOCKWORK ZONE OF THE WALL-ROCK HORNFELS AND IN THE VEIN BRECCIA, OCCURRING AS A MINERAL OF THE REPLACEMENT MINERALISATION OF THE VEIN-TYPE EPITHERMAL GOLD DEPOSIT IN THE DIAGENETIC FLYSCH ROCK AND RELATED METASOMATIC ZONE. SOME BASIC BUILDING ELEMENTS (Al, Ca AND Sr) AND TRACE ELEMENTS (Fe, Mn, As, Bi, Cu, Ga, Pb, Tl, U AND Zn) ARE PRESENT IN DISTINCTIVELY HIGH RATIOS

Oxides (%)	Instrument (XRF)	Sample	Elements	Instrument (ICP-AES)	Sample
	Detection limits (%)	Rhodonite occurring in metasomatic zone		Detection limits	Rhodonite occurring in metasomatic zone
SiO ₂	0.01	67.01	–	–	–
Al ₂ O ₃	0.01	0.37	Al	0.01 %	0.20
Fe ₂ O ₃	0.01	0.97	Fe	0.01 %	0.68
CaO	0.01	6.77	Ca	0.01 %	4.75
MgO	0.01	0.36	Mg	0.01 %	0.04
Na ₂ O	0.01	0.05	Na	0.01 %	< 0.01
K ₂ O	0.01	0.05	K	0.01 %	0.03
Cr ₂ O ₃	0.01	0.01	Cr	1 ppm	< 1
TiO ₂	0.01	< 0.01	Ti	0.01 ppm	< 0.01
MnO	0.01	18.61	Mn	5 ppm	> 100000
P ₂ O ₅	0.001	0.010	P	10 ppm	< 10
SrO	0.01	0.01	Sr	1 ppm	23
BaO	0.01	< 0.01	Ba	10 ppm	10
LOI	0.01	5.33			
Total	0.01	99.55			
			Ag	0.5 ppm	< 0.5
			As	5 ppm	40
			Be	0.5 ppm	0.6
			Bi	2 ppm	11
			Cd	0.5 ppm	< 0.5
			Co	1 ppm	1
			Cu	1 ppm	11
			Ga	10 ppm	50
			La	10 ppm	< 10
			Mo	1 ppm	< 1
			Ni	1 ppm	< 1
			Pb	2 ppm	66
			S	0.01 ppm	< 0.01
			Sb	5 ppm	9
			Sc	1 ppm	< 1
			Th	20 ppm	< 20
			Tl	10 ppm	40
			U	10 ppm	60
			V	1 ppm	2
			W	10 ppm	< 10
			Zn	2 ppm	142

- either as substitutional point defects or microphases¹⁶. The representative Anatolian rhodonite sample was analyzed for major oxides using XRF and for trace elements using ICP-AES (Table-1). The sample which was presented in this study is the representative sample. In fact, it was really analyzed five rhodonite samples; however the average of them was stated as the representative sample. The results are given comparatively in Table-1. The analyses reveal that some cations, such as Al, Ca, Sr, Fe, Mn, As, Bi, Cu, Ga, Pb, Tl, U and Zn are present in remarkably high ratios contrasting the instrumental detection limits. It can be concluded that during rhodonite formation, a rich element migration was present in the metasomatic zone. The XRD, XRF and ICP-AES results all indicate that the Anatolian rhodonite has a rich silica content and also some cation constituents. It is well known that the mineral rhodonite has a formula from MnSiO₃, (Mn,Fe)SiO₃ or (Mn,Ca,Fe)SiO₃. When considered chemical analyses, chemical composition of the Anatolian rhodonite should be formulized as (Mn,Ca,Fe)

SiO₃, even though the presence of quartz inclusions in this rhodonite do not affect its Ca and Fe content. It is proposed that results from the atomic substitutions of Mn by Ca and Fe^{6,10}. These structures contain the same basic features, in that Mn, Ca and Fe ions are octahedrally coordinated, with octahedra occurring in discontinuous sheets. Silica tetrahedra are arranged in chains with a repeat unit of five tetrahedra⁷.

Scanning electron microscope (SEM) photos obtained using two different techniques provide some individual illustrations of the Anatolian rhodonite sample. The first single photo, which was obtained using the BSE (back secondary electron) technique, is the scanning electron microscope (SEM) image showing the atom contrasts in the sample (Fig. 3). In this photo, with a 150x magnification, the condensed fields where atoms have a large atomic number and are consequently heavier are seen as white plots while areas where atoms have a lower atomic number are seen as black and/or greyish plots. According to this, the white plots on the SEM photo of the Anatolian

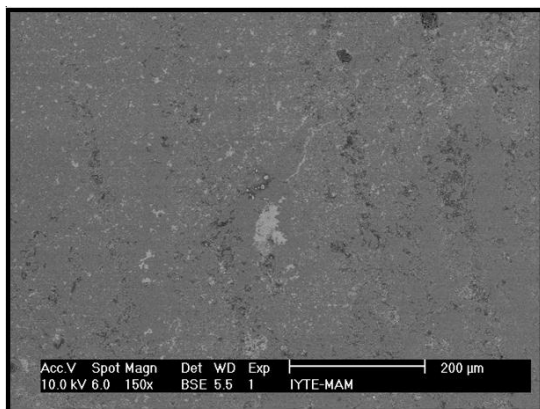


Fig. 3. Scanning electron microscope (SEM) image, obtained using the BSE (back scattered electron) technique to show the atom contrasts. The condensed fields where atoms have a large atomic number and are consequently heavier are seen as white plots, while areas where atoms have a lower atomic number are seen as black and/or greyish plots. Accordingly, the white plots on the image may be attributed to the presence of Fe, Mn and Ca atoms whereas the blackish and greyish plots may be attributed mainly to the presence of Si and O atoms

rhodonite can be ascribed to the presence of Fe, Mn and Ca atoms. In contrast, the blackish and greyish plots can be ascribed mainly to the presence of Si and O atoms and the others. The second group of SEM images are the series of photos which were obtained using the secondary electrons technique to show the submicron structure in the sample (Fig. 4). In these photos, with magnifications ranging from 150x-100.000x, respectively, it can be seen that the inner structure includes many different grain sizes, indicating a typical metasomatic replacement mineralization formation¹⁴.

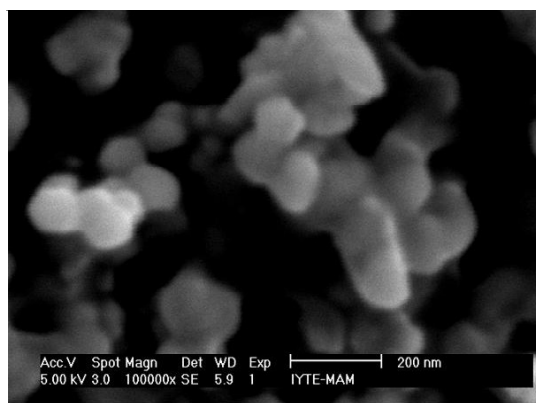
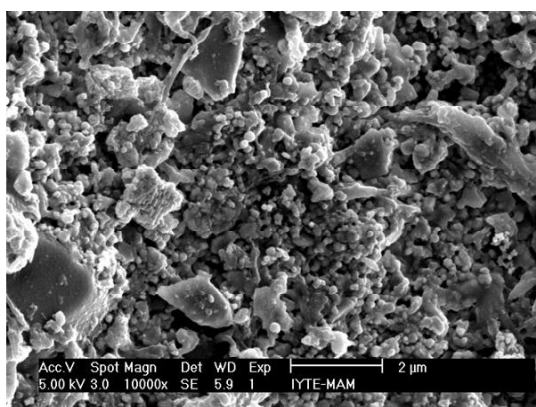
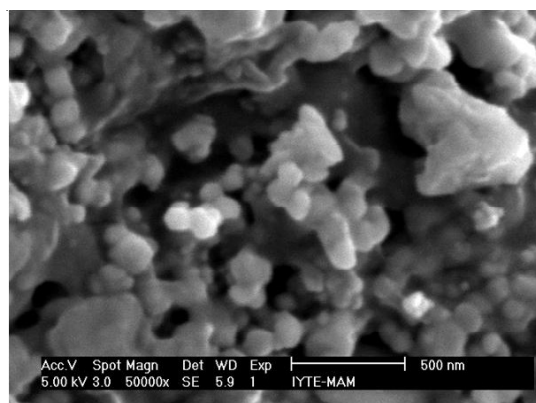
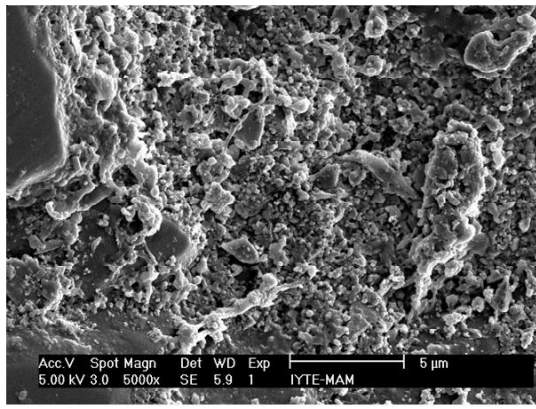
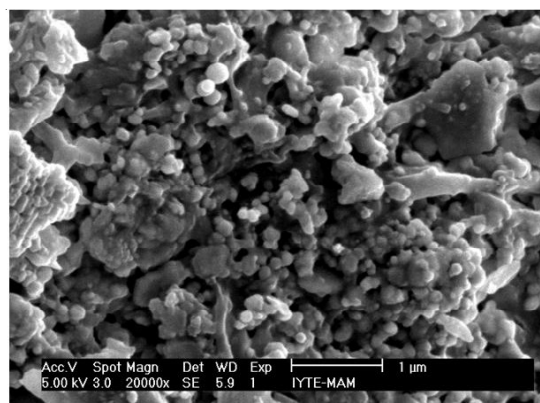
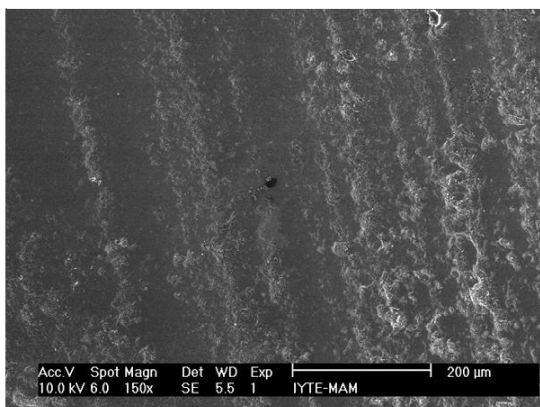


Fig. 4. Scanning electron microscope (SEM) images with magnifications ranging from 150x-100.000x, respectively, obtained using the SE (secondary electrons) technique to show the submicron structure. A heterogenic inner structure including large number cations with different grains sizes can be seen, indicating a metasomatic replacement mineralisation occurrence. Crystallinity, melting point and structural stability are strongly influenced by the reduction of particle grain size

For analysis of spectral luminescence emissions¹⁷, cathodoluminescence AC measurements at energies of 14 and 24 keV and frequencies from 9-900 Hz following electron irradiation at room temperature and cathodoluminescence DC measurements at 24 keV energy were performed on the Anatolian rhodonite samples. Cathodoluminescence spectra were excited using an electron beam with energies of 14 and 24 keV directed on to a spot of 1 cm diameter with a beam currents of 1 mA. Since electron beams can give us different spectra when different acceleration voltage and varying frequencies were used. The graphical patterns of the spectral emissions were given by Gaussian fitting^{15,18}. As seen in Figs. 5 and 6,

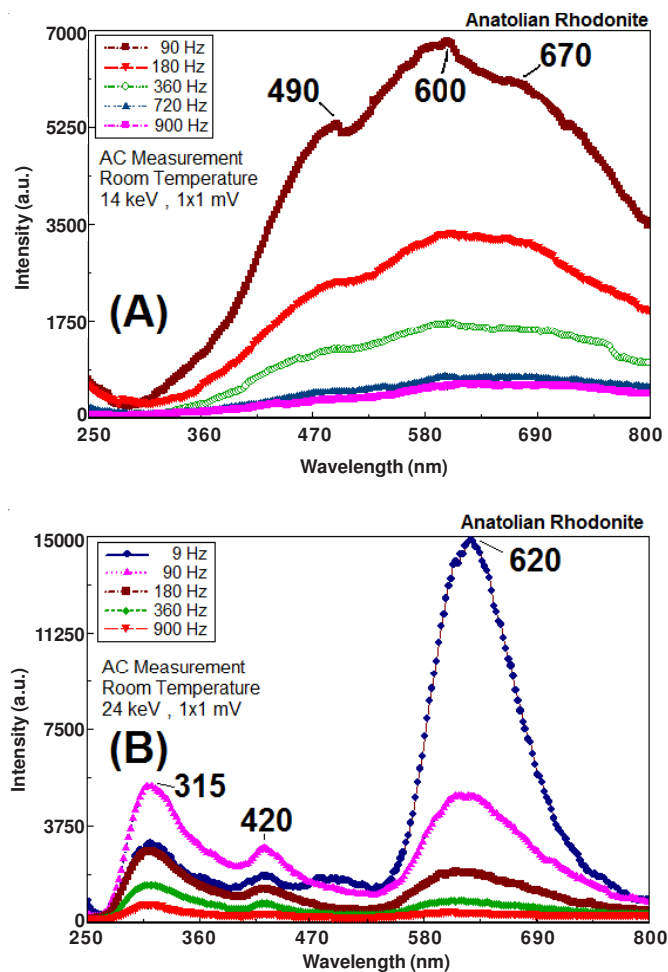


Fig. 5. Gaussian fitting of the cathodoluminescence AC (alternating current) experimental data of the rhodonite sample, at energies of 14 keV (A) and 24 keV (B). There exist three major spectral emissions at 14 keV, the dominant one being in the middle visible wavelength region (nearly yellow) at about 600 nm (A). In addition, there exists one major spectral emission at 24 keV, being in the visible wavelength region between yellow and orange at about 620 nm (B)

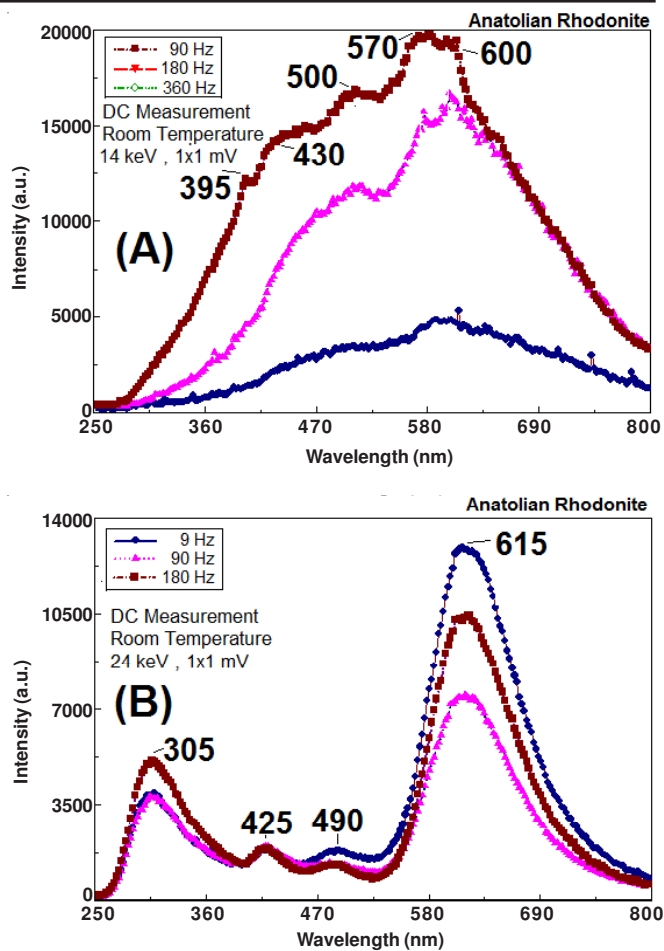


Fig. 6. Gaussian fitting of the cathodoluminescence DC (direct current) experimental data of the rhodonite sample, at energies of 14 keV (A) and 24 keV (B). There exist two major spectral emissions at 14 keV, being in the middle visible wavelength region (nearly yellow) at about 570 and 600 nm (A). In addition, there exists one major spectral emission at 24 keV, being in the visible wavelength region between yellow and orange at about 615 nm (B)

cathodoluminescence spectra from both AC measurements and DC measurements display similar patterns in the silica-rich Anatolian rhodonite samples. However, these samples, which occurred as an element of the secondary hydrothermal replacement mineralization paragenesis of the vein-type epithermal gold deposit in the Menderes-Izmir region of Turkey, consist of the unusual major components of SiO₂ (67.01 %), MnO (18.61 %), CaO (6.77 %), Fe₂O₃ (0.97 %), Al₂O₃ (0.37 %) and MgO (0.36 %), as well as a lot of trace elements (Table-1). Therefore, the samples display some distinctive spectral luminescence emissions (Table-2). Since, cathodoluminescence spectra are produced by excitation of electron beams. This excitation relate to chemical contents.

TABLE-2
CHARACTERISTIC EMISSION BANDS IN THE CATHODOLUMINESCENCE (CL) SPECTRA OF MASSIVE MASSES OF THE ANATOLIAN RHODONITE FROM THE MENDERES-IZMIR REGION IN TURKEY

Emission	Possible origin	Defect
Around 600 nm dominant band	*Substitutional Fe, Mn, As, Bi, Cu, Ga, Pb, Tl, U and Zn	Extrinsic lattice defect (impurity)
Around 500 nm	*Self-trapped exciton	Intrinsic lattice defect (structural imperfections)
Around 400 nm	*[SiO ₄ /M ²⁺] centre, *[AlO ₄ /M ²⁺] centre, M ²⁺ = Ca ²⁺ , Mg ²⁺	Extrinsic lattice defect (impurity)
Around 300 nm	*Nonbridging oxygen deficient centres with several precursors (i.e., hydroxyl group, peroxy linkage) *Oxygen vacancy	Intrinsic lattice defect (structural imperfections)

Accordingly, Gaussian fitting of the cathodoluminescence AC graphics of the samples at 14 keV energy and frequencies of 90 and 180 Hz (Fig. 5A) indicates that there are three major spectral emissions, the dominant one being in the middle visible wavelength region (nearly yellow) at about 600 nm. Additionally, two lesser emission lines occur in the longer visible wavelength region (nearly red) at about 670 nm and in the shorter visible wavelength region (nearly blue) at about 490 nm. In contrast, the cathodoluminescence data at 24 keV energy and frequencies of 9 and 90 Hz (Fig. 5B) indicate that one distinctive spectral emission in the visible wavelength region between yellow and orange at about 620 nm is present. A minor emission also exists in the shorter visible wavelength region (nearly lavender-blue) at about 420 nm and another minor one appears in the ultraviolet wavelength region at about 315 nm.

Gaussian fitting of the cathodoluminescence DC graphics at energies of 14 keV and 24 keV (Fig. 6) of the samples is similar to the AC graphics regarding their wavelength positions and intensities although their values are higher. It can be seen that the most distinctive emissions are produced at the lowest frequencies. These emissions from the longer visible wavelength region to the ultraviolet wavelength region are at about 600, 570, 500, 430 and 395 nm for 14 keV and 90 Hz (Fig. 6A) and at about 615, 490, 430, 425 and 305 nm for 24 keV and 9 Hz (Fig. 6B).

Lastly, the thermoluminescence glow curves of the Anatolian rhodonite sample after heating by X-ray for different irradiation times (10, 20 and 30 min)²¹ in the temperature range from 50-400 °C were taken (Fig. 7). The thermoluminescence spectrum generates two main peaks. They were observed at about 143 and 300 °C. Even if raised to the maximum dose, the behaviour of the thermoluminescence curves remains nearly stable, but their intensities increase. These data seem to be different to the previously reported data³. This difference may be attributed to electron transitions in the structure of the Anatolian rhodonite. It is well-known that for many thermoluminescence materials it appears that truly isolated trapping and recombination centres are an exception rather than a rule²⁰.

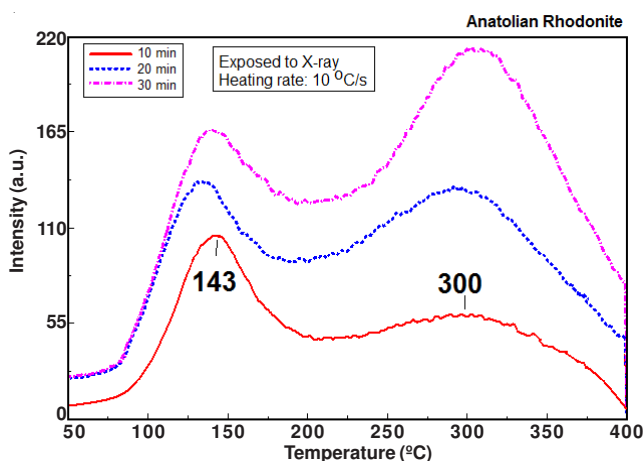


Fig. 7. Thermoluminescence (TL) spectra showing the glow curves of the rhodonite sample, which when exposed to different irradiation times, produced two main peaks at about 143 and 300 °C. Even if raised to the maximum dose, the behaviour of the thermoluminescence curves remains nearly stable, but their intensities increase. The glow peaks are caused by the trapped carriers which are produced during sample processing

In addition, in order to reveal the limits of the Anatolian rhodonite, it is necessary to observe the becoming pale of the pinkish natural colour of the sample. The Anatolian rhodonite was heated to over 700 °C. The result of additional heating of the sample was that the pinkish coloured rhodonite became blackish when heated over 600 °C in air. This result is similar to those of Brazilian rhodonite samples. Paiao and Watanabe⁹ stated that Brazilian rhodonite decays under heating up to 900 °C; it was reduced by 80 % of its original colour saturation at this temperature and consequently, the pink coloured natural rhodonite, when heated in air, starts becoming black⁹ at ca. 600 °C. Since, it is probable that there is a change in the oxidation state of the manganese ion.

Investigations of Anatolian rhodonite occurrences using X-ray diffractometry (XRD), scanning electron microscopy (SEM), bulk and trace element analyses (XRF and ICP-AES), cathodoluminescence and thermoluminescence spectroscopy indicated that various luminescence emission bands can be ascribed to different extrinsic defects (impurities) and intrinsic defects (structural imperfections)^{2,6,16} (Table-2).

It was revealed that the particular cathodoluminescence and thermoluminescence spectral emissions of the Anatolian rhodonite samples are due to the presence and even the relative abundance of certain chemical components derived from the hydrothermal alteration of the host rocks, which consequently serve to identify the provenance of the rhodonite and the paleo-temperature conditions in the stockwork zone of the wall-rock hornfels¹⁴ and the vein breccia in the region. Dominant cathodoluminescence emission including many emission peaks appearing at the yellow-orange region around 600 nm suggest that the Anatolian rhodonite may have arisen from a host with relatively lower levels of the basic building elements (Mg, Na, K, P and Ba) and consequently is richer in free silica and calcium, *i.e.*, it is of a more "neutral" character geochemically. However, some transition and rare earth elements (Fe, Mn, As, Bi, Cu, Ga, Pb, Tl, U and Zn) are significantly elevated (Table-1). The presence of the dominant cathodoluminescence band suggests that relatively higher levels of the transition elements (Table-2) can be attributed to a complicated hydrothermal system in the region. Consequently, the gem-quality Anatolian rhodonite occurs in an epithermal environment with a paleo-temperature condition of about 300 °C (according to thermoluminescence spectrum, Fig. 7) in response to rather sharp changes in solution chemistry caused by cooling and sudden increases in pH. During the secondary rhodonite and other related mineral occurrences, homogenization temperatures of 200-300 °C have been stated to reflect emplacement of ore distant from inferred magmatic heat in an epithermal environment¹⁴.

A similar cathodoluminescence study on quartz samples was published by Götze and his colleagues. This review study stated some very important results since it proved that luminescence spectroscopy could be used widely in geosciences and technical applications. One of the most important fields of application of quartz cathodoluminescence was the ability to reveal internal structures, growth zoning and lattice defects in quartz crystals not discernible by means of other analytical techniques. Other fields of investigation were the modal analysis of rocks, the provenance evaluation of clastic sediments,

diagenetic studies, the reconstruction of alteration processes and fluid flow, the detection of radiation damage and investigations of ultra-pure quartz and silica glass in technical applications¹⁶. Other similar genesis studies on various other minerals have also been reported^{15,17-19}.

Crystallinity, melting point and structural stability are strongly influenced by the reduction of particle grain size⁴. The change in the properties of grain particles is mainly produced by two factors: these are the increase in the surface to volume ratio and the change in electronic structure of the material due to the quantum confinement effect. As the particles become smaller, the surface/volume ratio and the surface states increase and therefore, reduce the excited emission *via* nonradiative surface recombination. This reveals that surface states are very important to the physical properties, especially the optical properties, of grain particles^{16,18}. The study of the surface states or trapping states is no less important than the design for quantum confinement. As the fluorescence quantum efficiency of grain particles is quite low, sensitive means are needed for luminescence measurement and to study the surface behaviour. Hence, the dominant cathodoluminescence emissions in the about yellow region of the Anatolian rhodonite are due to extrinsic defects, but the relatively minor cathodoluminescence emissions in the green, blue and ultraviolet regions are due to intrinsic defects (Table-2). Hence, it can be stated that the dominant cathodoluminescence emissions are due to the increasing amounts of tetrahedral character with increasing electron density resulting from the presence of the trace elements given in Table-1, taking into consideration the increased ionic character of the Si-O bond in the alkali silicate. Finally, the Anatolian rhodonite becomes more Ca-rich, less distorted and more ionic in character.

Conclusion

Spectral luminescence emissions, mainly cathodoluminescence following electron irradiation and thermoluminescence after heating by X-ray irradiation can be used as an indicator of the provenance and paleo-temperature conditions of replacement mineralization yields. The presented Anatolian rhodonite data emphasize the advantages and great potential of cathodoluminescence in several fields of research of secondary hydrothermal replacement mineralisation formation occurring in vein-type epithermal gold deposits in diagenetic flysch rock and related metasomatic zones as a result of geological field study.

XRD, XRF and ICP-AES results reveal that the Anatolian rhodonite has a rich silica content and also some cation constituents. In addition, there is a difference between atomic substitutions and the formation of different mineral phases. Therefore, the massive Anatolian rhodonite occurrence has a rich α -quartz silica phase, making it slightly different from crystalline rhodonite mineral occurrences in other worldwide localities. Indeed Anatolian rhodonite is unusual mass. Thus, it is original. It is proposed that these differences are due to the some atomic substitutions of Mn by Si, Ca and Fe.

Cathodoluminescence spectra of the Anatolian rhodonite mineral were obtained using measurements with alternating current (AC) at energies of 14 keV and 24 keV as well as

direct current (DC) at energies of 14 keV and 24 keV and with various frequencies up to 900 Hz. However, the highest intensities appear at the lowest frequencies, namely as 9, 90 and 180 Hz, respectively. The cathodoluminescence graphics indicate that the mineral which occurred in the replacement mineralization through the metasomatic zone includes many extrinsic and extrinsic defects. ICP-AES analysis suggests that, because of the presence and the unusual abundance of some major components (SiO₂, MnO, CaO, Fe₂O₃, Al₂O₃ and MgO), some basic building elements (Al, Ca and Sr) and some trace elements (Fe, Mn, As, Bi, Cu, Ga, Pb, Tl, U and Zn), these crystalline defects can be ascribed mainly to chemical impurities, but also to structural imperfections in the Anatolian rhodonite samples.

Particular cathodoluminescent spectral emissions from rhodonite may indicate the presence and even the relative abundance of certain chemical components derived from the hydrothermal alteration of surrounding rocks, which consequently serve to identify the provenance of the rhodonite.

The whole thermogram of the Anatolian rhodonite occurrence exhibits a complex structure in the form of a broad curve indicating the distinctive thermoluminescence glow curves, which serve to clarify the paleo-temperature conditions in the metasomatic environment. The change of thermoluminescence is consistent with that of the surface fluorescence. It is reasonable to consider that the thermoluminescence of the grain particles is correlated to the surface state.

In addition, it was observed that as a result of additional heating of the sample to over 700 °C in air, the pinkish coloured silica-rich rhodonite becomes blackish when heated to over 600 °C in air.

ACKNOWLEDGEMENTS

The author thanks to Prof. Dr. Nurdogan CAN, Asst. Prof. Dr. Rabia KIBAR, Asst. Prof. Dr. Ahmet ÇETIN and Asst. Dr. Yasemin TUNCER ARSLANLAR from Celal Bayar University, Manisa-Turkey for obtaining of cathodoluminescence and thermoluminescence measurements of rhodonite samples. In addition, thanks to Instructor Helen Margret MORAN-ÇAGLAR from Dokuz Eylül University, Izmir, Turkey, Foreign Languages School, for proof-reading the article.

REFERENCES

1. W.V. Maresch and A. Mottana, *Contribut. Mineral. Petrol.*, **55**, 69 (1976).
2. H. Narita, K. Koto and N. Morimoto, *Mineral. J. Sapporo*, **8**, 329 (1977).
3. R.A. Robie, J.S. Huebner and B.S. Hemingway, *Am. Mineral.*, **80**, 560 (1995).
4. F. Pertlik and R. Zahiri, *Monatsh. Chem.*, **130**, 257 (1999).
5. R.B. Cook, *Rocks Minerals*, **80**, 264 (2005).
6. F. Liebau, *Acta Crystallogr.*, **10**, 761 (1957).
7. D.R. Peacor and N. Nuzeki, *Z. Kristallogr.*, **119**, 98 (1963).
8. L.R. Pinckney and C.W. Burnham, *Am. Mineral.*, **73**, 798 (1988).
9. J.R.B. Paiao and S. Watanabe, *Phys. Chem. Mineral.*, **35**, 535 (2008).
10. P.G. Manning, *Can. Mineral.*, **9**, 348 (1968).
11. D.R. Peacor, E.J. Essene, P.E. Brown and G.A. Winter, *Am. Mineral.*, **63**, 1137 (1978).
12. W.R. Nelson and D.T. Griffen, *Am. Mineral.*, **90**, 969 (2005).
13. A. Baba and T. Güngör, *Environ. Geol.*, **41**, 621 (2002).
14. T. Oyman, F. Minerci and Ö. Piskin, *Ore Geol. Rev.*, **22**, 35 (2003).

15. P.D. Townsend and A.P. Rowlands, In eds.: M. Pagel, V. Barbin, P. Planc and D. Ohnenstetter, Information Encoded in Cathodoluminescence Emission Spectra, Cathodoluminescence in Geosciences, Springer, Berlin, pp. 41-57 (2000).
16. J. Götze, M. Plötze and D. Habermann, *Mineral. Petrol.*, **71**, 225 (2001).
17. D. Habermann, *Mineral. Petrol.*, **76**, 247 (2002).
18. D.J. Marshall, Cathodoluminescence of Geological Material, Unwin Hyman, Boston, p. 345 (1988).
19. J. Götze, *Freiberger Forschungshefte*, **A172**, 128 (2000).
20. S.W.S. McKeever, Thermoluminescence of Solids, Cambridge University Press, Cambridge, p. 392 (1985).
21. A.J.J. Boss, *Radiat. Measur.*, **41**, 545 (2007).
22. ASTM, Index (Inorganic) to the Powder Diffraction File; ASTM Special tech. Pub. 48-M2, American Society for Testing and Materials, Philadelphia, p. 244 (1963).
23. C.M. Clark and R.T. Downs, *J. Geosci. Educ.*, **51**, 76 (2001).
24. RRUFF, Database of Raman Spectroscopy, X-Ray Diffraction and Chemistry of Minerals, via <http://rruff.info/> (2011).
25. WEBMINERAL, Minerals Arranged by X-Ray Powder Diffraction via <http://webmineral.com/MySQL/xray.php> (2011).